Supplement of Atmos. Chem. Phys., 20, 6273–6290, 2020
https://doi.org/10.5194/acp-20-6273-2020-supplement

Atmospheric Chemistry and Physics
Open Access

Supplement of

Direct links between hygroscopicity and mixing state of ambient aerosols: estimating particle hygroscopicity from their single-particle mass spectra

Xinning Wang et al.

Correspondence to: Xiaofei Wang (xiaofeiwang@fudan.edu.cn) and Xin Yang (yangxin@fudan.edu.cn)

1. ATOFMS particle numbers and concurrent CPC number concentrations during the HTDMA-ATOFMS characterization.

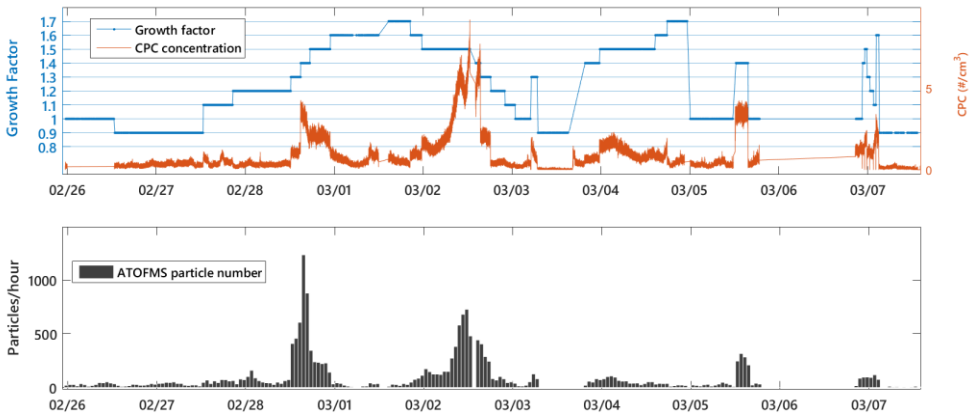

Figure S1. Particle number concentrations in the outflow of HTDMA as measured by CPC and the prescribed GFs in HTDMA-ATOFMS characterization (upper). The lower panel is the concurrent ATOFMS particle numbers (hour resolution).

2. Particle hit rates and detection efficiencies at different growth factors

As shown in Figure S2, ATOFMS hit rates were higher for particles of low hygroscopicity (GF <1.3). For more hygroscopic mode (GF >1.4) particle hit rates lie in 10-20% range. This variation of hit rate is probably caused by the different particle compositions at different growth factors. As previous found in a ATOFMS study, the coating of secondary species on particles can reduce the ionization efficiencies and lower particle hit rate (Hatch et al., 2014). This is consistent with the present results that more hygroscopic particles tend to produce stronger secondary peaks.

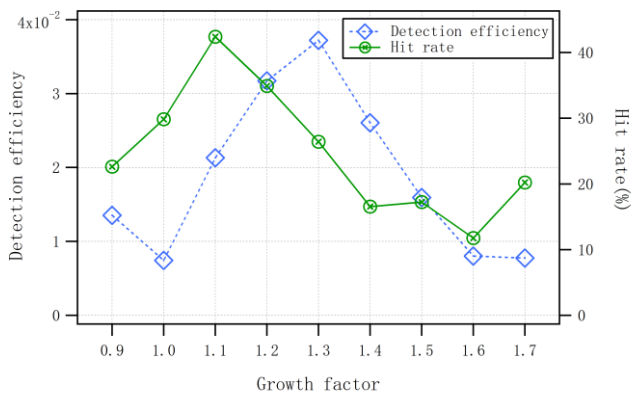

Figure S2. Particle hit rates at different growth factors in the HTDMA-ATOFMS experiment.

3. The application of 0.5 power treatment to peak intensities

We took 0.5 power of mass peak intensities in the estimation of GF. This treatment was applied to both the HTDMA-ATOFMS and ambient particle data before the evaluation of particle similarity. It is known that ATOFMS mass peak intensities are affected not only by composition abundance in particles, but also by their ionization efficiencies in ATOFMS. The ATOFMS is generally more sensitive to metallic compositions than organics, resulting disproportionate large peaks of metals to reflect their actual concentrations in particles. We suppose the 0.5 power treatment of mass peak areas can partly solve the bias of ATOFMS toward different compositions, since this treatment reduce larger peaks more rapidly than smaller peaks. Similar treatment (logarithm of peak areas) of ATOFMS data was proposed in prior literature (Rehbein et al., 2012). In ATOFMS data analysis the peak relative intensities were also used. Relative intensities are the normalized intensities by total peak area in a spectrum. This normalization removes the amplitude of peak intensity vector but the overall shape of a spectrum is not changed.

The application of 0.5 power treatment is not just based on speculation. We find it gave better results in the estimated hygroscopicity. We carried two rounds of GF estimations in which the pretreatment was either included or not. In figure S3 the two distributions of estimated GF using 0.5 power treatment or not are compared. As shown in figure, the hygroscopicity distribution without treatment suggests abnormal shape, with an extra mode of GF=1.35 which was inconsistent with HTDMA observations in this area. As a comparison, with the 0.5 power treatment to peak intensities and we obtained a smoother hygroscopicity distribution with regular shapes, which agrees well with the HTDMA data of ambient particles. We note that in the two estimations the dataset and algorithm are identical with the only difference of the pretreatment. This fact suggests that the 0.5 power treatment could indeed be used to improve hygroscopicity estimation.

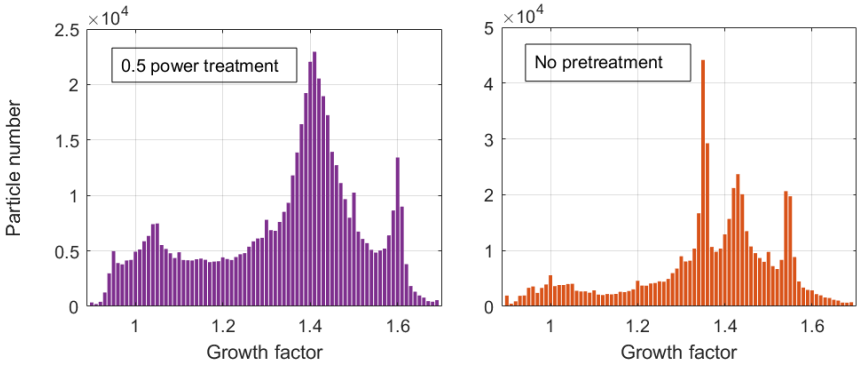

Figure S3. The estimated particle hygroscopicity distribution with (left) and without (right) taking 0.5 power of peak intensities.

4. The distribution of matching similarities between HTDMA-ATOFMS and ambient particles

In this preliminary study, we set a similarity threshold at 0.7 (dot product) in matching particles, similar as the ART-2a algorithm requested. Particles with matching similarities <0.7 were excluded from analysis in estimated GF. We noted that the 0.5 power pretreatment to peak intensities lowered the matching dot products (79.4% of matching similarities >0.8, average 0.86) compared with situations without treatment (95.8% of matching similarities >0.8, average 0.94), since peaks of smaller intensities have increased weights in the similarity evaluation. In Figure S4 we present the distribution of matching similarities with 0.5 power treatment in this study. The data suggests that the majority of ambient ATOFMS particles (96.2%) were matched with HTDMA-ATOFMS particles with similarity > 0.7.

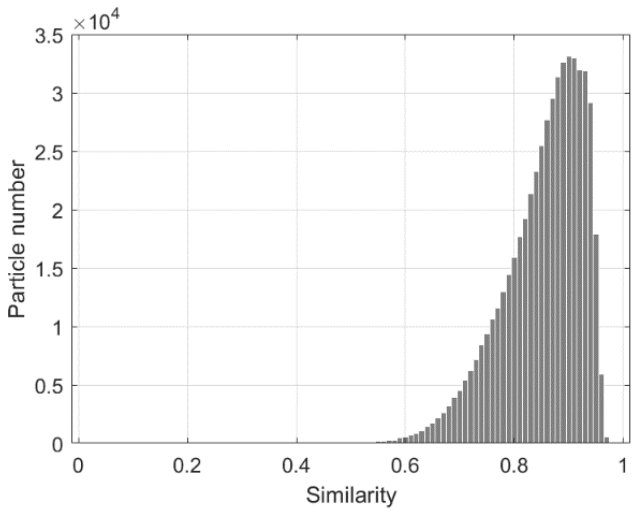

Figure S4. The distribution of matching similarities between ambient ATOFMS and HTDMA-

ATOFMS particles.

5. Variations of estimated GF in different matching criteria

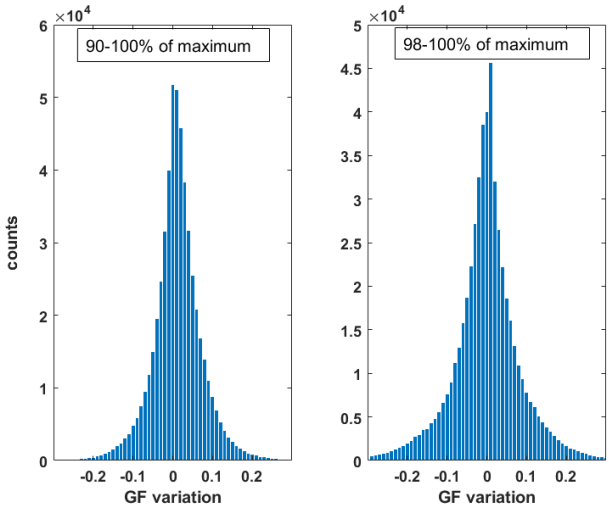

Figure S5. Distributions of the GF changes in estimated GF using different matching criteria. The reference GF data is generated from criteria of 95-100% maximum dots product.

6. Peak intensity variations of as a function of GF for EC particles

The nitrate and sulfate were internally mixed in most of the EC particles. Secondary nitrate and sulfate are the major contributor to the hygroscopic growth due to their high hydrophilicity (Gysel et al., 2007;Aggarwal et al., 2007). The signal intensities of nitrate, sulfate and ammonium in EC particle spectra are summarized in Figure S2. Noted that ATOFMS is not a quantitative method and the area of mass peaks cannot be used directly to infer chemical quantity in single particles. However the variations of peak intensities based on statistics of many particles can be used to demonstrate their relative trends (Gross et al., 2000;Hatch et al., 2014;Pratt et al., 2009). In Figure S2 we present secondary peak intensities of nitrate (-62 NO_3^-), sulfate (-97 SO_4^-), ammonium (+18 NH_4^+) and EC related peaks of -24C_2^- -25C_2H^-, -36C_3^- as a function of hygroscopicity. As shown in the figure, nitrate intensity increases within the GF <1.2 range, and then a roughly stable level was reached in the GF>1.2 range (MH mode). This feature is also present in sulfate and ammonium peaks. The signal intensity trends demonstrate the aging process of fresh EC particles with the formation of secondary nitrate, sulfate and ammonium. The signal intensity trends obtained here are comparable

with the previous study, although some differences were noticed (Herich et al., 2008;Wang et al., 2014). Herich et al. similarly found the nitrate intensity increased with GF in GF <1.3 range before a plateau was reached (Herich et al., 2008). However, in that study the sulfate intensity did not show clear trend with GF, which is not consistent with the present data. The aging process of EC particles is indicated by the intensity variations of other peaks in the negative spectra. As shown in the right panels in Figure S2, the negative peaks at -24C_2^- -25C_2H^-, -36C_3^-, which are stronger in spectra of fresh EC particles (Suess, 2002), gradually decrease as the GF increase, suggesting their potential application to indicate the degree of aging of EC particles.

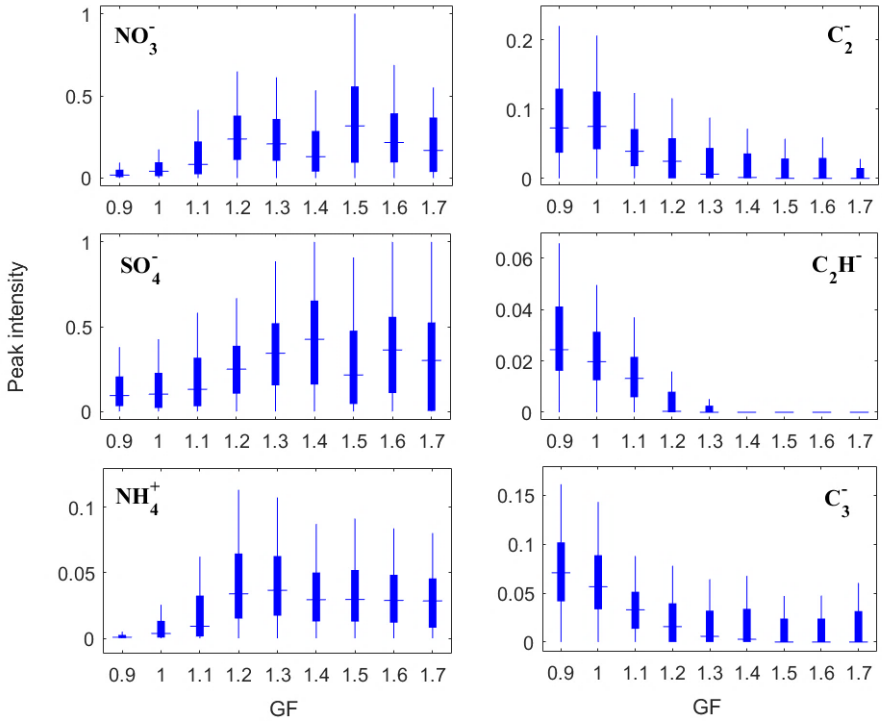

Figure S6. Statistics of relevant peak intensities in EC particle spectra as a function of GF. The statistics from bottom to top for each GF: minimum, 25th percentile, median, 75th percentile, maximum.

7. Mass spectral similarities between particles in different GF groups.

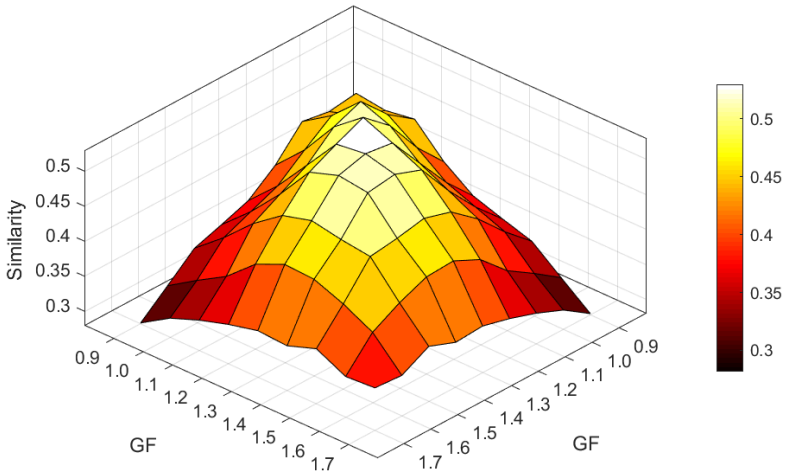

Figure S7. The diagram showing the average mass spectra similarities between each pair of GF groups (GF 0.9-1.7).

8. Average mass spectra of GF=1.6 mode particles.

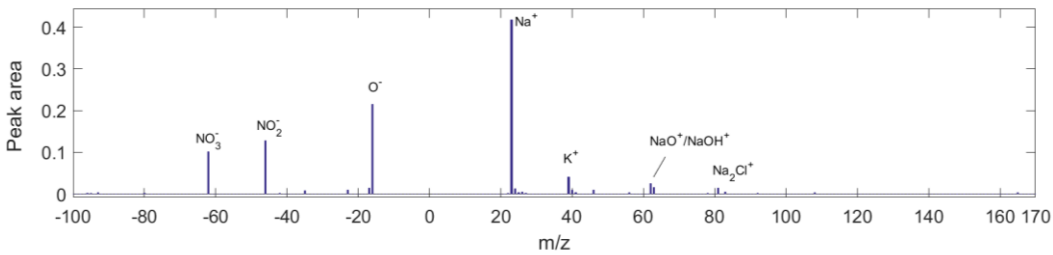

Figure S8. The average mass spectra of particles in GF 1.6 mode

9. Airmass back trajectories of P1-P4 periods

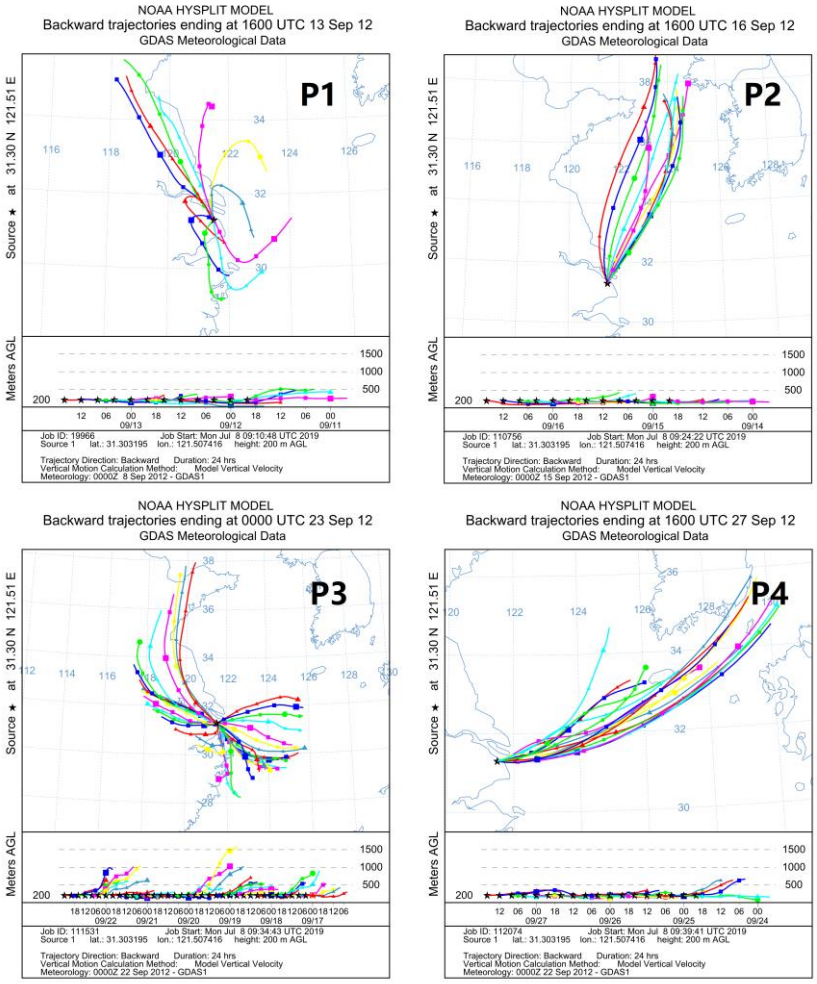

Figure S9. The 24-hour backward trajectories during P1 - P4 periods of the sampling site (by HYSPLIT model).

10. Particle number contributions in different areas in Peak intensity-GF distribution diagram.

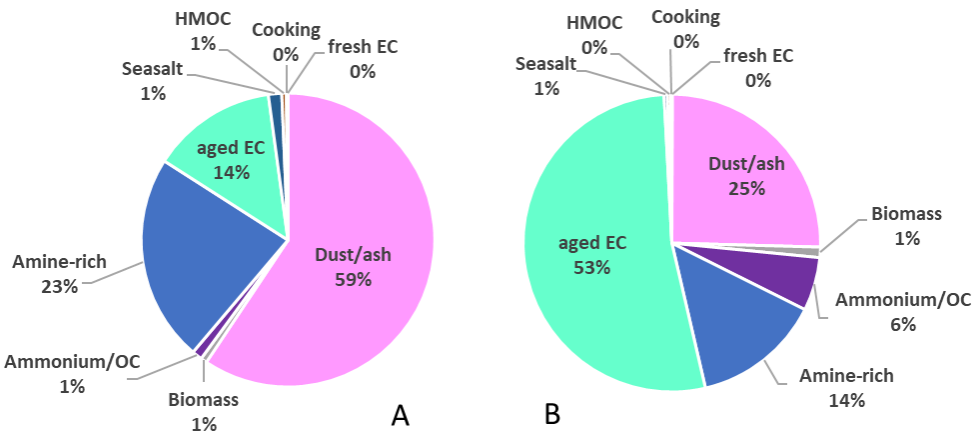

Figure S10. Number contributions of particle types to A and B region as indicated in Figure 10 in the main text.

11. Peak intensity variations with the estimated GF of sea salt particles

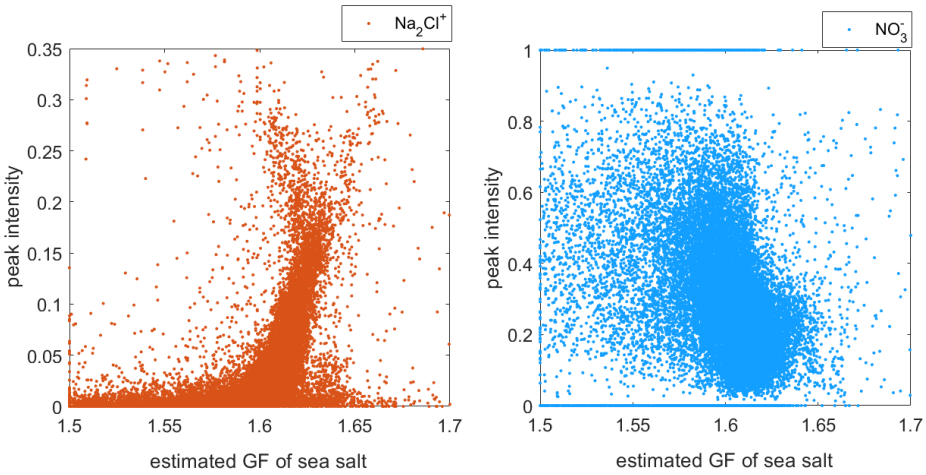

Figure S11. The correlation between mass peak intensities of sea salt particles with their estimated GF. Left panel shows the summarized peak intensities of Na_2Cl^- peak at m/z 81 and 83 and right panel shows the intensities of NO_3^-.

12. Visibility temporal variations at Hongqiao and Pudong airport during Sep-12 to Sep-28.

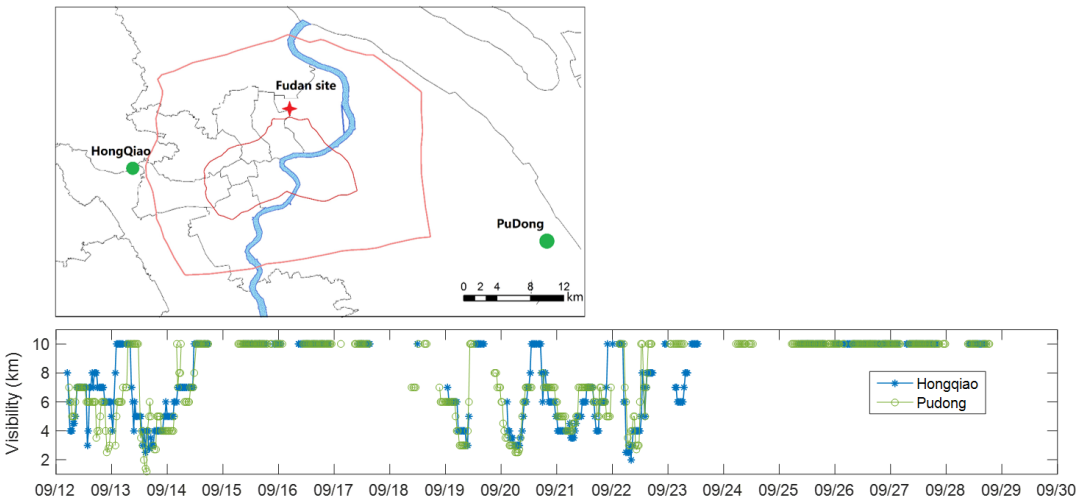

Figure S12. Temporal variations of visibility at Hongqiao and Pudong airport from Sep-12 to Sep-28,2012. The map shows the positions of Hongqiao, Pudong airport and the Fudan site.

13. Correlations between atmospheric visibility and PM concentration.

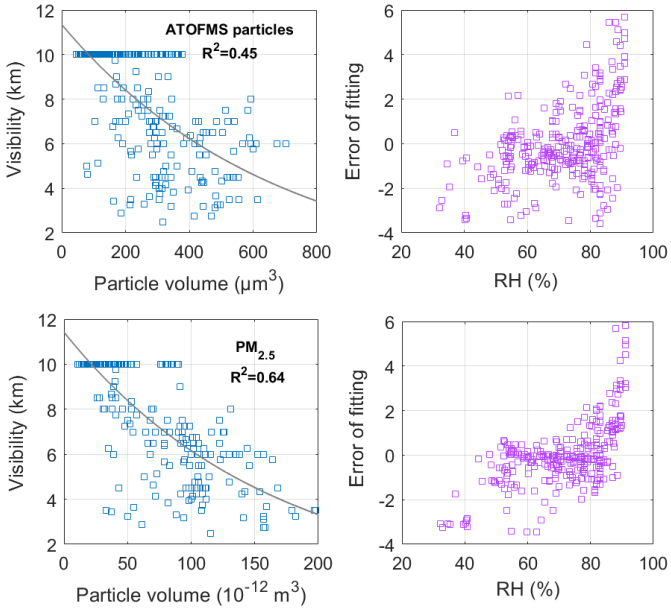

Figure S13. The left column shows the correlation between particle volume concentrations and visibility. The volume concentrations were calculated separately from ATOFMS particles and $PM_{2.5}$ concentrations. Right column shows the errors of fitted values from data as a function of ambient RH.

References

Aggarwal, S. G., Mochida, M., Kitamori, Y., and Kawamura, K.: Chemical closure study on hygroscopic properties of urban aerosol particles in Sapporo, Japan, Environmental Science & Technology, 41, 6920-6925, 10.1021/es063092m, 2007.

Gross, D. S., Galli, M. E., Silva, P. J., and Prather, K. A.: Relative sensitivity factors for alkali metal and ammonium cations in single particle aerosol time-of-flight mass spectra, Analytical Chemistry, 72, 416-422, 10.1021/ac990434g, 2000.

Gysel, M., Crosier, J., Topping, D. O., Whitehead, J. D., Bower, K. N., Cubison, M. J., Williams, P. I., Flynn, M. J., McFiggans, G. B., and Coe, H.: Closure study between chemical composition and hygroscopic growth of aerosol particles during TORCH2, Atmospheric Chemistry and Physics, 7, 6131-6144, 2007.

Hatch, L. E., Pratt, K. A., Huffman, J. A., Jimenez, J. L., and Prather, K. A.: Impacts of Aerosol Aging on Laser Desorption/Ionization in Single-Particle Mass Spectrometers, Aerosol Science and Technology, 48, 1050-1058, 10.1080/02786826.2014.955907, 2014.

Herich, H., Kammermann, L., Gysel, M., Weingartner, E., Baltensperger, U., Lohmann, U., and Cziczo, D. J.: In situ determination of atmospheric aerosol composition as a function of hygroscopic growth, Journal of Geophysical Research-Atmospheres, 113, D16213 10.1029/2008jd009954, 2008.

Pratt, K. A., Hatch, L. E., and Prather, K. A.: Seasonal Volatility Dependence of Ambient Particle Phase Amines, Environmental Science & Technology, 43, 5276-5281, 10.1021/es803189n, 2009.

Suess, D. T.: Single particle mass spectrometry combustion source characterization and atmospheric apportionment of vehicular, coal and biofuel exhaust emissions, Ph.D., University of California, Riverside, United States -- California, 377-377 p. pp., 2002.

Wang, X. N., Ye, X. N., Chen, H., Chen, J. M., Yang, X., and Gross, D. S.: Online hygroscopicity and chemical measurement of urban aerosol in Shanghai, China, Atmospheric Environment, 95, 318-326, 10.1016/j.atmosenv.2014.06.051, 2014.